Predicting Tonal Noise of Full-Electric Propeller-Driven Aircraft in Outdoor Environments Using Low-Order Models

Yunus, F.; von den Hoff, B.; Snellen, M.

DOI
10.2514/6.2024-3418

Publication date
2024

Document Version
Final published version

Published in
30th AIAA/CEAS Aeroacoustics Conference (2024)

Aeroacoustics Conferences
June 4-7, 2024, Rome, Italy
30th AIAA/CEAS Aeroacoustics Conference (2024)

10.2514/6.2024-3418

Predicting tonal noise of full-electric propeller-driven aircraft in outdoor environments using low-order models

Furkat Yunus*, Bieke von den Hoff†, and Mirjam Snellen‡
Aircraft Noise and Climate Effects section, Control and Operation Department, Delft University of Technology, Delft, The Netherlands

This paper presents a low-order method for assessing tonal noise from full-electric propeller-driven aircraft during outdoor operations. A high-fidelity numerical simulation and several outdoor measurements were performed to validate the approach and identify the dominant noise source. Outdoor measurements involve constant-altitude level flight and three take-off flights. The low-order method focuses exclusively on blade and hub geometry, while the numerical simulation considers propeller blades and the spinner. Comparison of outdoor measurements, numerical simulations, and low-order model predictions reveals the propeller as the primary noise source for the specified aircraft configuration, with negligible interactions with the airframe. The study further demonstrates that during take-off flights noise levels at higher harmonics are more sensitive to variations in propeller disk angles of attack. These findings underscore the importance of addressing propeller noise in full-electric propeller-driven aircraft. Additionally, the paper emphasizes the practical application of the low-order approach for evaluating the aircraft's noise footprint during take-off flights, providing crucial insights for early design stages.

Nomenclature

a	=	axial velocity induction coefficient
b	=	tangential velocity induction coefficient
b_c	=	blade sectional airfoil chord length, m
B	=	number of blades
D	=	propeller diameter, m
B_D	=	chord-to-diameter ratio, b_c/D
$J_{mB-k}(x)$	=	Bessel function of order $mB-k$ and argument x
R	=	radial distance along the propeller blade, m
$\boldsymbol{x}$	=	receiver position vector with (x, y, z) components in a Cartesian coordinate system, m
S	=	distance between propeller hub and receiver location, $\sqrt{x^2+y^2+z^2}$, m
c_0	=	ambient sound speed, ms^{-1}
Δr	=	width of a blade element
r_t	=	propeller tip radius; $D/2$,m
ΔT	=	sectional thrust, N
ΔQ	=	sectional torque, N m
V_∞	=	free stream velocity, ms^{-1}
z_0	=	non-dimensionalized blade radius, R/r_t
m	=	acoustic harmonic number
k	=	loading harmonic number
k_x	=	dimensionless chordwise wave number
k_y	=	dimensionless spanwise wave number
M_x	=	flight Mach number, V_∞/c_0
M_t	=	tip Mach number, $\Omega r_T/c_0$

*Postdoctoral researcher, Control & Operation Department, f.yunus@tudelft.nl.
†PhD candidate, Control & Operation Department, b.vondenhoff@tudelft.nl.
‡Professor, Control & Operation Department, m.snellen@tudelft.nl.

M_r = $\sqrt{M_x^2 + M_t^2}$, helicoidal tip rotational Mach number
k_m = $\frac{mB\Omega}{c_0}$, harmonic wave number
t_b = thickness to chord ratio
Ω = angular speed, rads^{-1}
$\hat{\Psi}_{Fk}$ = Frequency domain source function
α = airfoil angle of attack, rad
α_{disk} = propeller disk angle of attack, rad
β = blade geometric pitch angle, rad
θ = receiver angle relative to flight direction, arccos (x/S), rad
ϕ = tangential angle (z/y) and flow induction angle, rad
θ', ϕ' = angles θ and ϕ relative to propeller shaft axis, rad
ζ = helix angle, rad
ρ_0 = ambient density, kgm^{-3}

I. Introduction

According to the NASA Regional Air Mobility report [1], noise and potential emissions are key factors influencing local communities' resistance to new airports and expanded air services, such as urban air mobility (UAM). The electrification of the propeller-driven aircraft offers a range of benefits, such as reduced maintenance requirements, lower carbon emissions, and quieter takeoffs and landings [2]. Although full-electric propeller-driven (FEPD) aircraft are quieter than those powered by combustion engines, considering low-altitude operation over densely populated areas still poses significant challenges to reducing aircraft noise further. Consequently, effective mitigation of propeller-generated noise becomes a foundational requirement in the pursuit of quieter electric aircraft design [3].

Propeller noise can be categorized into two components: tonal noise, which includes thickness noise (resulting from volume displacement by the propeller blades) and loading noise (caused by steady and unsteady forces acting on the blade during rotation), and broadband noise, which emerges from two sources: turbulence being carried past the trailing edge of the blade (known as self-noise) and the unsteady turbulence interaction with the blade (also known as turbulence ingenstion noise) [4]. This study focuses only on the tonal component associated with thickness and steady loading noise.

Over the years, numerous methods have been devised for assessing tonal noise generated by propellers. These methods exhibit a hybrid nature and can be categorized into two distinct approaches: the high-fidelity (HF) approach and the low-order (LO) approach. The HF approach utilizes the acoustic analogy and requires flow data obtained using HF CFD simulation as input to resolve the acoustic sources [5]. As the HF CFD simulation requires extensive computational resources, the HF approach is not considered to be coupled with a design or operational optimization routine in an industrial context to minimize the propeller noise. The LO approach, on the other hand, couples an aerodynamic solver with an acoustic one [6]. The aerodynamic solver typically uses the blade element momentum theory (BEMT) to calculate the aerodynamic forces at radial stations along the blade radius based on two-dimensional airfoil lift and drag coefficients obtained by coupled panel/boundary-layer models like XFOIL [7] and *Opty∂B*-BEMT [5] or wind tunnel experiments. Several previous studies [8–10] have compared the predictive accuracy of BEMT against CFD results for a selection of propellers, focusing on aerodynamic efficiency and accuracy. Their collective findings indicate that BEMT demonstrates comparable accuracy to CFD, especially at lower advance ratio velocities [10]. Notably, the BEMT method has shown consistent reliability in generating results that align closely with experimental data while maintaining a minimal computational expense [11, 12]. Highlighting the aeroacoustic efficiency and accuracy of the LO approach, Casalino et al. [5] conducted a benchmark activity for low Reynolds number propeller aeroacoustics. Their study involved comparisons between wind-tunnel experiments, HF simulations utilizing the lattice-Boltzmann very large eddy simulation (LB/VLES) method, and a LO approach. The LO workflow notably achieved accurate predictions of forces and tonal noise. In a similar vein, Yunus et al. [6, 13] compared a LO approach with the frequency-domain acoustic formulation from Hanson [14–17] against the time-domain compact dipole/monopole formulation of FW-H acoustic analogy and HF CFD simulation coupled with acoustic analogy using the Farassat 1A formulation. Their research demonstrated that the LO approach, employing the frequency domain formulation, can conveniently predict propeller tonal noise in forward flight conditions, delivering a significant speedup compared to its time-domain counterpart. Kvurt et al. [18, 19] recently introduced a LO approach to predict propeller tonal noise and extended it to include

contributions of unsteady loading noise during hover conditions. Their method integrates BEMT with XFOIL and a frequency-domain acoustic formulation, significantly enhancing the analysis of propeller tonal noise.

In all works mentioned above, however, the LO approach is validated against either fully controlled wind tunnel measurements or HF simulations and other LO models. Thus, the range of applicability of the LO approach to predict the noise signature of FEPD aircraft operating in an outdoor environment has never been investigated. Furthermore, recent LO approaches have primarily concentrated on idealized conditions such as hovering or forward flight, wherein the incoming flow aligns with the propeller's axial direction, thus supporting the uniform inflow assumptions inherent in the BEMT approach. Consequently, the suitability of LO approaches for predicting tonal noise from propellers during take-off flights, where the incoming flow does not align with the propeller axis, has not been thoroughly investigated, particularly in outdoor operations. Nevertheless, it is pertinent to note that the acoustic solver utilized in this study is based on the later work of Hanson [15, 16, 20], which can account for acoustic effects of non-axial flow conditions typically encountered during take-off flights. Moreover, the hypothesis that the propeller itself is the main noise source for a FEPD aircraft has not been properly verified in the previous works. Hence, the objective of this research is twofold: i) to assess the range of applicability of the LO model to predict the tonal noise of FEPD aircraft operating in an outdoor environment considering level-flight and take-off flights; ii) to investigate the primary source of noise by comparing results obtained from a HF approach, which considers only the propeller geometry, with outdoor experimental measurements conducted on the full-scale aircraft.

The remainder of the paper is organized as follows: Section II presents an overview of the LO model. Section III contains a description of the experimental and numerical case setup. Section IV presents the results. Finally, the conclusion is given in Section V.

II. Overview of the LO approach

In this work, a LO propeller noise prediction solver (LOPNOR) is developed. This solver consists of three parts. The first part is a preprocessing module. This module reads propeller geometry in standard triangle language (STL) file format, discretizes the blade geometry along its span, and extracts sectional airfoil coordinates at each blade section, as illustrated in the left panel of Fig. 1. The airfoil coordinates at each section are formatted following the XFOIL convention, i.e., airfoil coordinates are ordered from the trailing edge to the leading edge and back to the trailing edge. Hence, XFOIL can directly read the generated airfoil coordinates without the manual modification of airfoil coordinates. For given ranges of Reynolds numbers (R_e) and angle of attack α covering the whole range of radial variation, the solver runs XFOIL internally to calculate the aerodynamic polars for each combination of Reynolds number and angle of attack. This procedure generates 2D meshes of sectional lift and drag coefficients, $C_l(Re, \alpha)$ and $C_d(Re, \alpha)$, respectively. In this study, α ranges from $-16°$ to $16°$ with $2°$ increment, and several values of the Reynolds number covering the whole range of radial variation are considered. The post-stall lift and drag coefficients are computed using the Viterna & Corrigan approach [21]. At the end of this procedure, calculated sectional lift and drag coefficients are then stored into the disk with user-defined file names to avoid repeating the XFOIL calculation for any adjustments irrelevant to the airfoil polar data.

The aerodynamic forces and coefficients, namely C_l and C_d, along the blade radial stations are determined in the second step by executing the BEMT procedure. The BEMT is a hybrid method that combines the basic principles from both blade element and momentum approaches. The momentum approach assumes that the flow passing through the propeller forms a well-defined streamtube, where the propeller is replaced by an actuator disk (see Fig. 2). The actuator disk is divided into multiple annuli in the momentum approach. An annulus located at a distance R from the rotational axis and having a width of Δr has an area of $\mathrm{d}A = 2\pi R\Delta r$. The sectional thrust on an annulus is the product of the mass flow rate through the annulus and the total change in velocity between far upwind from the disk and far downwind of the disk, which is twice the induced velocity at that section ($V_{a3} = 2V_a = 2aV_\infty$). The axial velocity induction coefficient is denoted by a, and the axial velocity $V_x = V_\infty(1 + a)$. The mass flow rate over the annulus is $\mathrm{d}\dot{m} = \rho_0\,\mathrm{d}AV_x = 2\pi\rho_0 V_x R\Delta r$, which leads to the sectional thrust on the annulus

$$\Delta T = \mathrm{d}\dot{m}V_{a3} = 2\pi\rho_0 V_x R\Delta r V_{a3} = 4\pi\rho_0 V_\infty^2(1 + a)aR\Delta r. \tag{1}$$

To determine the forces at any blade radius, the blades are divided into radial elements of width Δr as illustrated in Fig. 2, where each blade element can be considered individually. Namely, the blade element theory considers that no forces act in the radial direction, so each element is subjected to two-dimensional flow [22]. This approach has good validity except near the blade tips. Nonetheless, an effective approximation of the impact of tip-loss on the inflow distribution is achieved through the utilization of Prandtl's tip-loss correction model, which is implemented in this study.

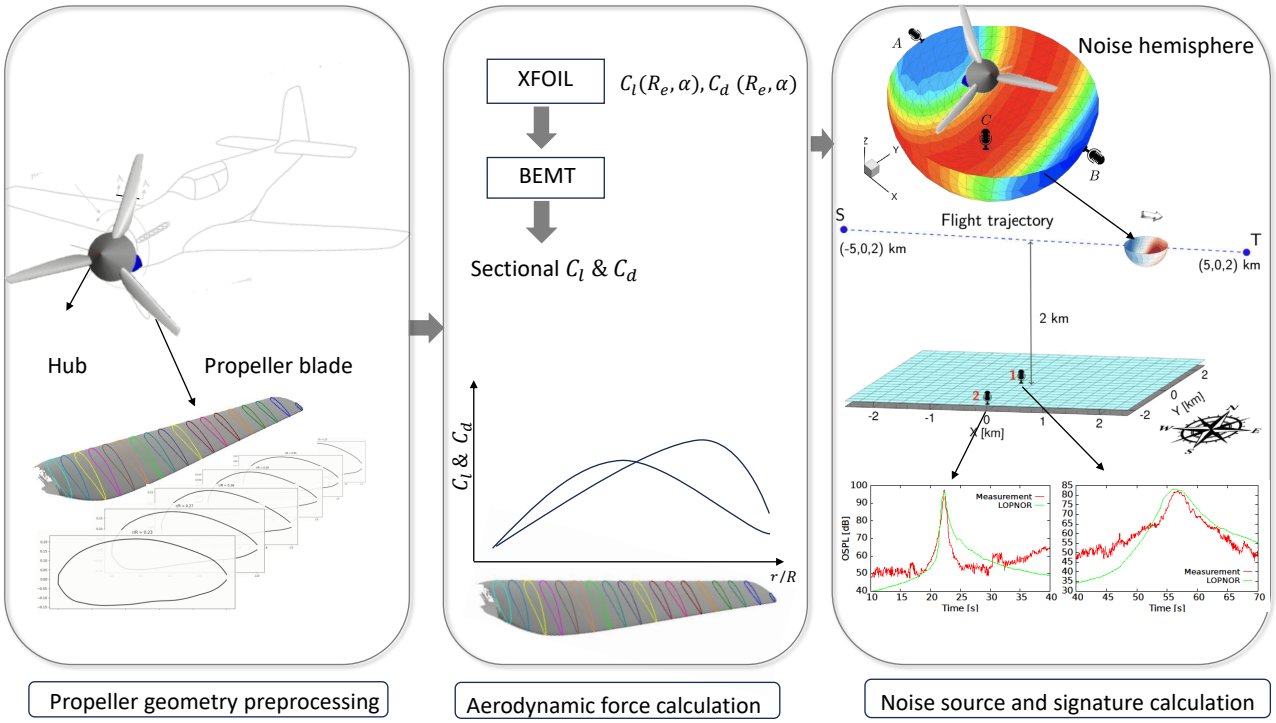

Fig. 1 An overview of computational procedures of the LO model.

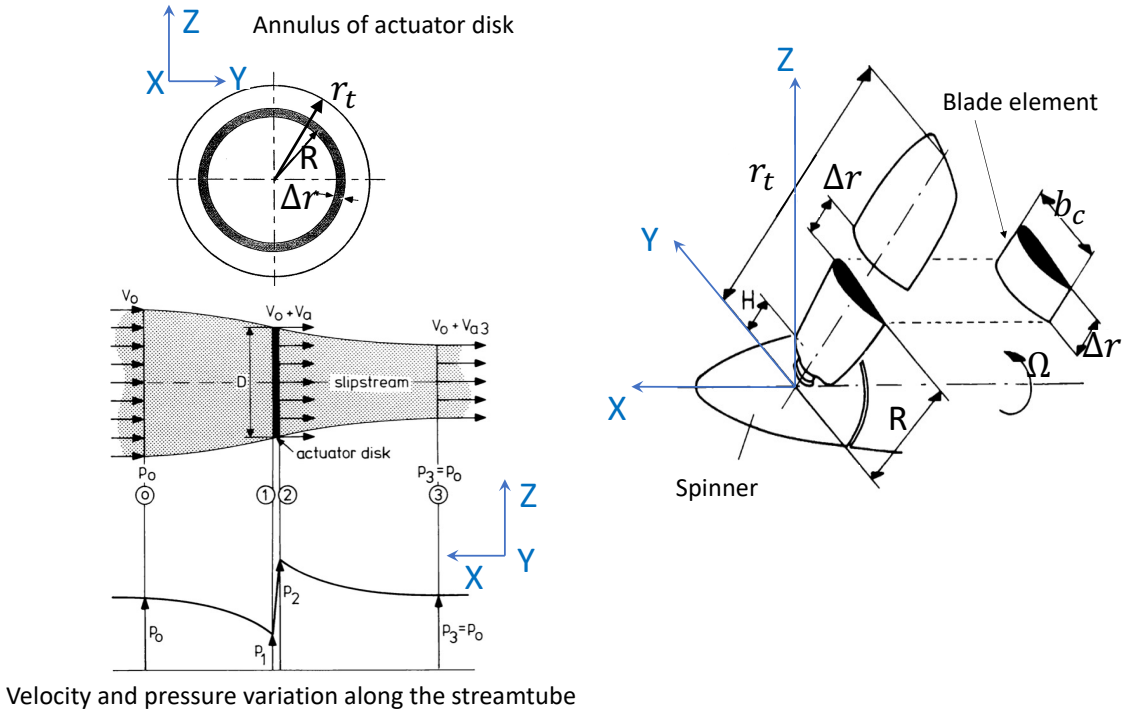

Fig. 2 The annulus of the rotor disk (top left) and a streamtube created by the propeller motion (bottom left) and blade element of a rotor (right) (adapted from [13]).

In the BEMT procedure, the sectional thrust and torque on an annulus of width Δr can be determined by establishing an equilibrium that reads:

$$\Delta T = 4\pi R\rho_0 V_\infty^2(1+a)a\Delta r = \frac{1}{2}\rho_0 V_1^2 b_c(C_l\cos\phi - C_d\sin\phi)B\Delta r, \tag{2}$$

$$\Delta Q = 4\pi R^3\rho_0 V_\infty\Omega(1+a)b\Delta r = \frac{1}{2}\rho_0 V_1^2 b_c(C_d\cos\phi + C_l\sin\phi)BR\Delta r, \tag{3}$$

where R is the radius of the blade section and b_c is the blade sectional chord, B is the number of blades, b is the azimuthal velocity induction coefficient ($V_t = \Omega R(1-b)$), $V_1 = \sqrt{V_x^2 + V_t^2}$ is the total velocity seen by every radial section and $\phi = tan^{-1}(V_x/V_t)$ is the flow induction angle. The local angle of attack as a consequence of the geometrical blade section pitch angle β and flow induction is $\alpha = \beta - \phi$. Upon determining the Reynolds number and angle of attack seen by the sectional airfoil, the associated lift and drag coefficients C_l and C_d are interpolated from the 2D meshes of $C_l(Re,\alpha)$ and $C_d(Re,\alpha)$ values established in the prior step. The overall thrust and torque generated by a single blade are then obtained by integrating the sectional thrust ΔT and torque ΔQ along the blade's radial direction. The thrust and torque coefficients C_T and C_Q are acquired by multiplying the thrust and torque by $1/(\rho_0\Omega\pi r_T^4)$ and $1/(\rho_0\Omega^2\pi r_T^5)$, respectively.

In the final stage, unlike the work by Kotwicz Herniczek et al. [17, 23] and Yunus et al. [6, 13], in which the ΔT and ΔQ are delivered as inputs for the acoustic calculation, in this work the aerodynamic force coefficients (C_l and C_d) at each blade section, along with the respective blade sectional areas, are inputted into the frequency domain acoustic formulation [20] for the computation of tonal noise. The loading $p'_L(\boldsymbol{x},\Omega)$ and thickness $p'_T(\boldsymbol{x},\Omega)$ components of the tonal noise read

$$p'_L(\boldsymbol{x},\Omega) = \frac{i\rho_0 c_0 B e^{ik_m S}}{4\pi(S/r_t)(1-M_x\cos\theta)}\sum_{k=-\infty}^{\infty} e^{i(mB-k)(\phi'-\pi/2)}\times\int_0^{r_t} M_r^2\hat{\Psi}_{Fk}(k_x)J_{mB-k}\left(\frac{mBz_0M_r\sin\theta'}{1-M_x\cos\theta}\right)dz_0, \tag{4}$$

$$p'_T(\boldsymbol{x},\Omega) = \frac{-\rho_0 c_0^2 B e^{ik_m S}}{4\pi(S/r_t)(1-M_x\cos\theta)}\sum_{k=-\infty}^{\infty} e^{i(mB-k)(\phi'-\pi/2)}\times\int_0^{r_t} M_r^2\hat{k_x}^2 t_b\hat{\Psi}_V(\hat{k_x})J_{mB-k}\left(\frac{mBz_0M_r\sin\theta'}{1-M_x\cos\theta}\right)dz_0. \tag{5}$$

where the angles θ' and ϕ' are given by the following relations with respect to propeller disk angle of attack α_{disk} [20, 23]

$$\cos\theta' = \cos\theta\cos\alpha_{disk} + \sin\theta\sin\phi\sin\alpha_{disk}, \tag{6}$$

$$\cos\phi' = \frac{\sin\theta}{\sin\theta'}\cos\phi. \tag{7}$$

The frequency domain source function is expressed as $\hat{\Psi}_{Fk}$, and it can be written in various forms. This work considers an expression of $\hat{\Psi}_{Fk}$ that is explicitly dependent on the aerodynamic coefficients, as advised by Hanson [20].

$$\hat{\Psi}_{Fk} = \frac{1}{2}(k_y C_{lk}\hat{\Psi}_{lk} + k_x C_{dk}\hat{\Psi}_{dk}). \tag{8}$$

$\hat{\Psi}_{Fk}$ is associated with the source functions Ψ, as previously elucidated by Hanson [14], through the following relation

$$\hat{\Psi}_{(\cdot)k} = \Psi_{(\cdot)k}e^{i(\phi_s+\phi_{FA})}, \tag{9}$$

where ϕ_s is the phase angle due to sweep and ϕ_{FA} is the phase shift associated with Face Alignment. In this study, parabolic thickness distribution and uniform lift distribution, as defined by Eq. (16)-(17) in Kotwicz Herniczek et al. [23], are utilized, following the recommendation of Magliozzi et al. [24]. The dimensionless wave numbers k_x and k_y, representing chordwise and spanwise dimensions, respectively, are determined according to Hanson [14]

$$k_x = \frac{2mBM_t}{M_r(1-Mx\cos\theta)}B_D, \quad k_y = \frac{2mB}{2M_r}\left(\frac{M_r^2\cos\theta - M_x}{1-M_x\cos\theta}\right)B_D. \tag{10}$$

The wavenumber $\hat{k_x}$ in Eq. 5 reads

$$\hat{k_x} = 2\left(\frac{mB-k}{z_0}\cos\zeta + \frac{mBM_r\cos\theta'}{1-M_x\cos\theta}\sin\zeta\right)B_D \tag{11}$$

where ζ is the helix angle which varies along the blade span. In a previous study by Hanson [14], the angle was denoted as the advance helix. However, Hanson argued in a subsequent study [20] that it could alternatively represent the blade twist angle or any other pertinent angle that varies along the blade span and is associated with the distribution of noise sources. In this study, the helix angle is specifically set to the blade twist angle.

The corresponding pressure time history at a receiver location $\boldsymbol{x}$, which combines the contributions of thickness and loading noise, can be determined using the following equation

$$p'(\boldsymbol{x},t) = \sum_{m=-\infty}^{\infty}[p'_L(\boldsymbol{x},\Omega) + p'_T(\boldsymbol{x},\Omega)]e^{-imB\Omega t} \tag{12}$$

Finally, it is worth noting that in this study, only the zeroth harmonic of loading, i.e., $k = 0$, is considered, as only the steady loading and thickness noise are taken into account.

III. Experimental and numerical setup

The outdoor experiment was carried out by N. S. L. Elbers and her research team. A comprehensive description of the experimental setup is available in her thesis [25]. For the sake of completeness, a brief overview of the setup is provided in the following section. For additional details, please consult [25].

A. Experimental setup

The experiment encompassed four measurements conducted on July 20, 2021, between 18:42 and 19:08 hours. The subject of the noise measurements was the Velis Electro. The Velis Electro is a FEPD two-seater aircraft manufactured by Pipistrel [26], notable for being the first of its kind to receive certification for short-range missions. It is particularly well-suited for pilot training. This aircraft is operated by the E-flight academy, which is the only electric flight school in the Netherlands, making it an ideal choice for pilot training. The Velis is equipped with the Pipistrel E-811-268MVLC, an EASA Type-Certified engine with a maximum take-off power (MTOP) of 57.6 kW and a maximum speed of 2500 RPM. [27]. The aircraft has the P-812 / 164-F3A Certified fixed pitch composite three blade propeller, which has a diameter of $D = 1.64$ m and rotates in clockwise direction when looking from the cabin (see Fig. 3a). Additional details regarding the aircraft and propeller geometry can be found in the type certification data sheet accessible on the EASA website [27] and N.S. L. Elbers' master thesis [25].

The outdoor measurements were conducted at Teuge International Airport in The Netherlands. During outdoor measurements, a microphone array with 64 microphones was deployed (refer to Fig. 4.3 in [25]). This study focuses on noise signals sampled from 8 microphones positioned at the array center. These microphones are placed on an acoustic foam, specifically Flamex 15, acting as a noise-absorbing material to minimize ground reflection effects (with no consideration for ground reflection during measurements). To further mitigate outdoor turbulence impacts on noise measurements, windshields are installed over the microphones.

In addition to the microphone array, two tools enhance the noise measurement process. A GoPro, positioned in the cockpit, records instrumentation details displaying flight speed (V_∞), RPM, and altitude (h). Simultaneously, a Garmin GLO global positioning system (GPS) sensor, connected to a smartphone via Bluetooth, records aircraft position using the myTracks GPS app. The collected GPS data is stored in files with .gpx and .kml formats, allowing seamless processing through Python or MATLAB in subsequent steps.

The meteorological data representing the weather conditions during the measurements were obtained through the Royal Dutch Meteorological Institute, KNMI, and are listed in Table 1. Teuge Airport does not have a KNMI station therefore the weather conditions from the closest station in Deelen are used.

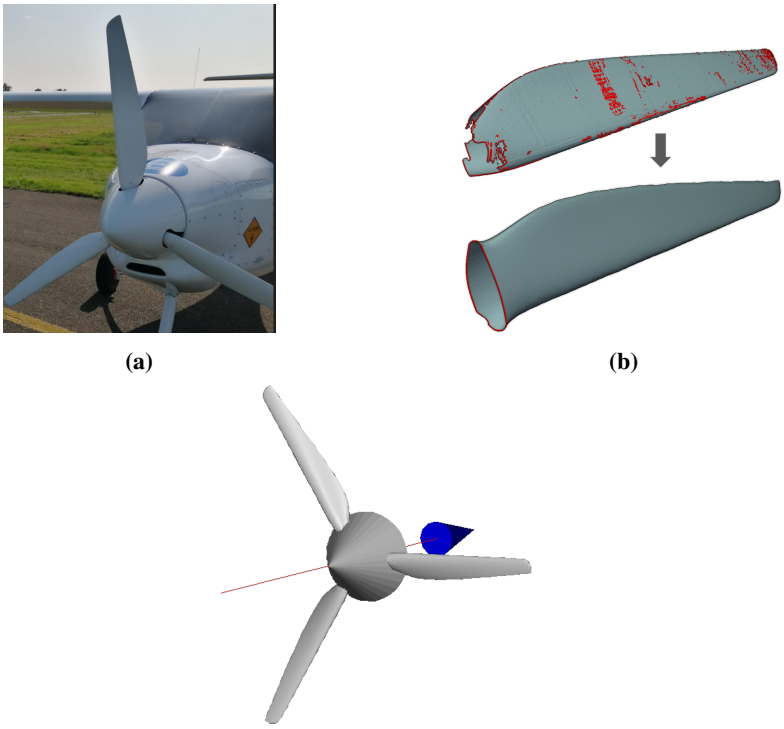

(a) **(b)** **(c)**

Fig. 3 (a) Close-up view of the propeller used in the outdoor measurements [25]. (b) Side view of 3D scanned blade geometry (top) and the same blade geometry with gaps filled and repaired (bottom). Red circles indicate holes on the surface of the blade geometry. (c) Digital copy of the propeller used in the CFD simulation.

Table 1 Weather conditions at Deelen Airport.

Parameter #	Value	Unit
Temperature (T)	19.5	°C
Pressure (P)	1021.7	hPa
Relative humidity (RH)	67	%
Wind direction (WD)	East	-
Wind speed (V_{wind})	1	m/s

B. Numerical setup

1. Digitization of propeller geometry

The digital copy of the propeller blade was acquired via 3D scanning using the FARO 3D scanner [28]. Comprehensive information about the scanner and the scanning process is available in [25]. The 3D scanner provides the blade's geometric data in STL file format. As illustrated in the upper panel of Figure 3b, the 3D-scanned blade geometry contains holes and gaps which are not desired for aerodynamic and acoustic analysis. To address this, a Python script is developed tailored to process the scanned blade geometry, resulting in the cleaned and mended blade geometry depicted in the lower panel of Figure 3b. The refined blade geometry is utilized within the digital environment for further analysis in the subsequent sections.

The HF numerical simulation is conducted using the HF CFD solver SIMULIA PowerFLOW based on the LB/VLES method coupled with FW-H acoustic analogy [29]. The noise source in the HF approach is predicted by employing the FW-H solver of SIMULIA PowerACOUSTICS on the scale-resolved flow data from PowerFLOW. The FW-H solver is based on a forward-time solution [30] of Farassat's formulation 1A [31]. The noise signals utilized in this study are computed using the solid surface formulation of the FW-H acoustic analogy, which considers the blade surface as the source. Casalino et al. [5] conducted a grid convergence study using the 3DS aeroacoustic workflow, examining various grid resolutions from coarse to fine and validating convergence by monitoring force and tonal noise at a medium resolution. This study leverages the same medium resolution within the same workflow to generate the HF simulation results, eliminating the need to repeat the grid convergence analysis.

C. Description of test cases

In total, four noise measurements were conducted. The distance h between the ground microphone and the aircraft as well as the rotational speed RPM were extracted from the GoPro video recording of the flight instrument for each measurement case where the aircraft flew overhead. Flight speed V_∞ was derived from GPS sensor data, which recorded the aircraft's position at one-second intervals. Further setup details of GoPro video recording in the cabin and GPS sensor configurations can be found in [25]. The propeller disk angle of attack α_{disk} is extracted from the GPS data. These values, corresponding to each Case, are listed in Table 2.

Table 2 Test matrix for the case study.

Case #	h [m]	V_∞ [m/s]	RPM	α_{disk} [deg]	J	Measurement	CFD
1	7.43D	41.7091	2500	0.0	0.6055	✓	✓
2	46.46D	31.0443	2430	5.6	0.4674	✓	-
3	24.16D	36.8442	2460	2.53	0.5480	✓	-
4	26.07D	36.1095	2440	2.67	0.5414	✓	-

The first Case pertains to a constant-altitude level flight, with the subsequent three Cases denoting take-off flights under specified operating conditions. Notably, the CFD simulation is performed only for the first Case. It's important to emphasize that this CFD simulation exclusively encompasses the propeller, including its blades and spinner, without accounting for any interaction between the propeller and the surrounding airframes in the analysis.

IV. Results

A. Noise spectrum

The validity of the proposed LO approach and whether the propeller itself is the dominant noise source are investigated by comparing the predictions from LO and HF approach against the outdoor measurements. The noise spectra of all three sets of signals are obtained by performing Fourier transformation with a 50% overlap, Hamming windowing, and a bandwidth of 6.1035 Hz. As shown in Fig. 4a, the HF approach shows good agreement with the

measurement at the first two harmonics of blade passage frequency (BPF). In the third and fourth BPF, the HF result captures well the trend of the measurement results with a slight overprediction of the corresponding tonal peaks. In contrast, the LO prediction shows favorable agreement with the measurement results all the way up to the sixth harmonics with a slight overprediction up to the fourth harmonics of BPF. At fifth harmonics, the decay of LO predictions is observed to occur at a faster rate in comparison to both the measurement and HF predictions. This phenomenon is likely attributed to the dominance of unsteady effects at higher harmonics, which are not encompassed within the LO approach. In other words, the LO prediction captures well the trend of the tonal noise at all its harmonics visible in the outdoor measurement results. Furthermore, a high degree of agreement is observed between the LO prediction and HF simulation results for up to the fifth harmonics of BPF. This comparison highlights the validity of the present LO approach in predicting tonal noise emitted by FEPD aircraft operating in outdoor environments. Additionally, the comparison results indicate that the propeller acts as the primary source of noise within the tonal frequency range, with discernible tonal peaks corresponding to the harmonics of the BPF above the broadband component. Within this frequency range, the influence of various aerodynamic interactions between the propeller and the airframes can be neglected during constant altitude level flight.

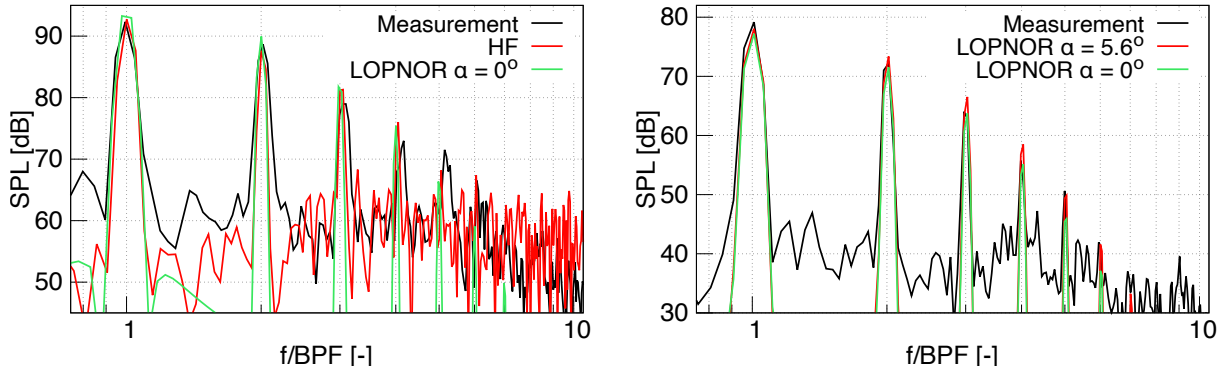

(a) Case 1: $h = 7.43D$, $RPM = 2500$. **(b) Case 2:** $h = 46.46D$, $RPM = 2430$.

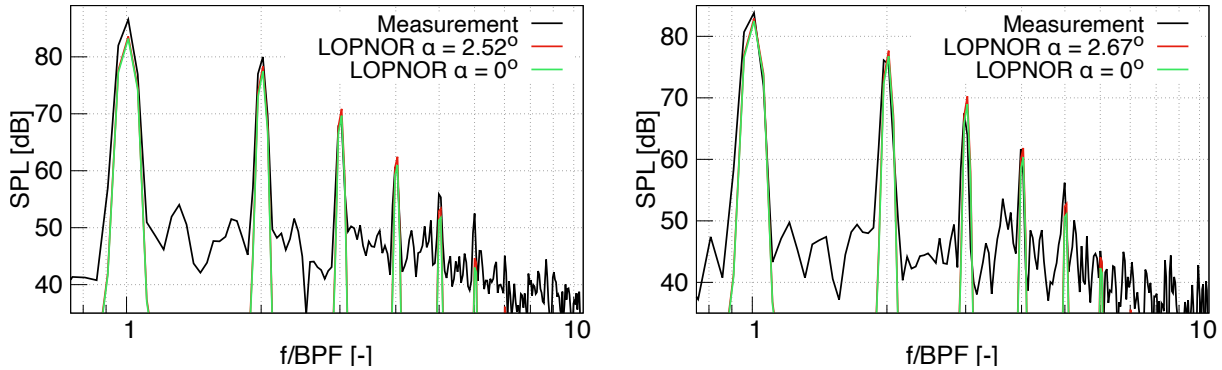

(c) Case 3: $h = 24.16D$, $RPM = 2460$. **(d) Case 4:** $h = 26.07D$, $RPM = 2440$.

Fig. 4 Comparison of the noise spectra calculated with the LOPNOR tool against outdoor measurements.

The applicability of the present LO approach to predict noise from FEPD aircraft during take-off flights, where the propeller operates with a non-zero α_{disk} relative to the flight direction, is investigated by comparing the LO predictions with outdoor measurements for Cases 2-4. In Case 2, as depicted in Fig. 4b, improved accuracy in higher harmonics is demonstrated by the LO prediction with α_{disk}, albeit with slight overprediction of the tonal peaks at the third and fourth harmonics. This improved accuracy at higher harmonics is attributed to the acoustic effects of $\alpha_{disk} \neq 0°$. The noise characteristics of a propeller operating at $\alpha_{disk} \neq 0°$ significantly differ from those at $\alpha_{disk} = 0°$, as elucidated in previous works [16, 20, 32, 33]. When operated at $\alpha_{disk} \neq 0°$, two primary mechanisms contribute to tonal noise: periodic variations in blade loading and asymmetric phase modulation of noise sources' strength. The latter, also known as the wobbling mode [16, 32], is purely acoustic and characterized by the periodic variation of the observer-source relative Mach number. Consequently, due to the purely acoustic effect of non-zero α_{disk}, when a propeller tilts away

from a ground receiver, as in take-off flights, noise levels at the receiver increase compared to the noise levels with zero α_{disk}. Hanson [20] demonstrated that the acoustic effect of non-zero α_{disk} is a dominant contributor to higher harmonics compared to the contribution from unsteady loading. This trend is confirmed by the enhanced prediction of tonal noise peaks at higher harmonics. Similar trends have been observed in Case 3 and Case 4. However, it is worth mentioning that the inclusion of a non-zero α_{disk} significantly improves the prediction accuracy for Cases 2-4, but it still underpredicts the tonal peaks at higher harmonics, particularly when α_{disk} is smaller, as in Case 3. This is possibly due to the non-axial inflow that induces unsteady loading, further contributing to increased noise levels at higher harmonics [20]. Hence, better prediction agreement at higher harmonics can be obtained by including unsteady loading effects, which will be studied in future work.

B. Time-level history of flyover noise

The computation of the time-level history of flyover noise follows similar approaches as those presented in previous works by the lead author [6, 34]. In these works, the noise signals are computed and stored on virtual microphones distributed over a hemisphere surrounding the aircraft. Subsequently, the noise signals are propagated towards the ground receiver, taking into account the emission time positions of the aircraft for a given flight trajectory.

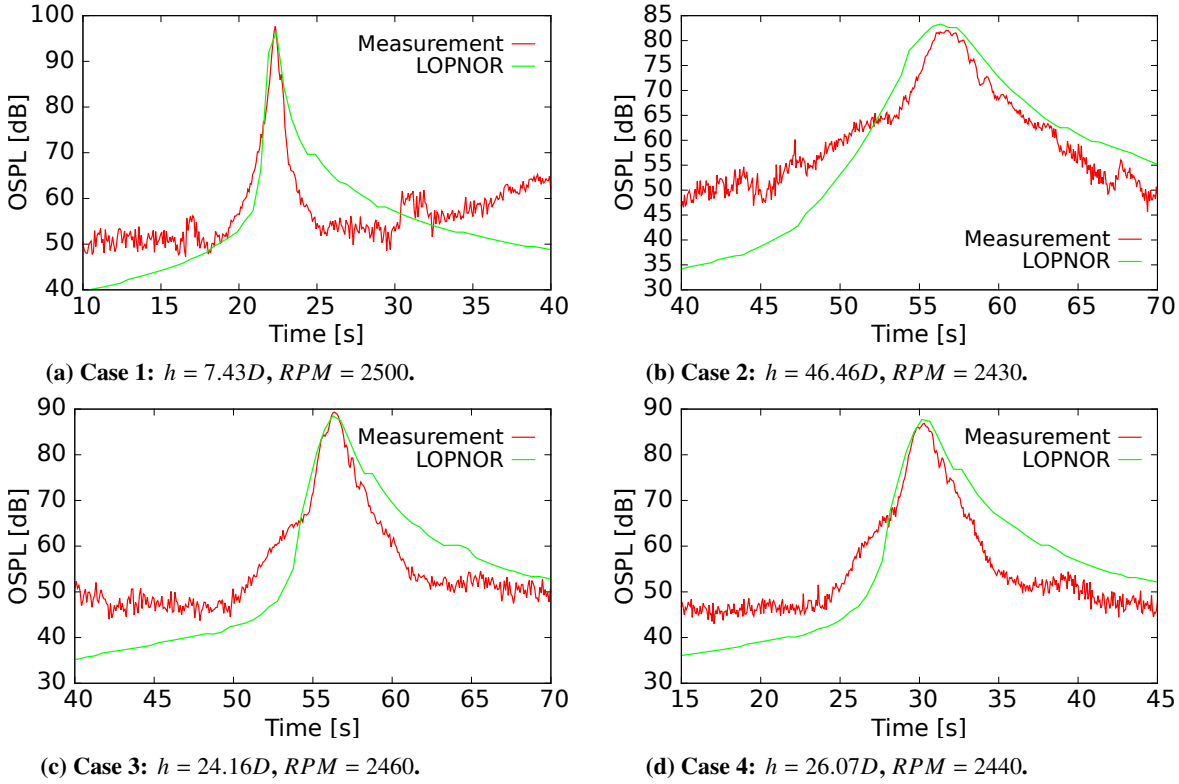

(a) Case 1: $h = 7.43D$, $RPM = 2500$.

(b) Case 2: $h = 46.46D$, $RPM = 2430$.

(c) Case 3: $h = 24.16D$, $RPM = 2460$.

(d) Case 4: $h = 26.07D$, $RPM = 2440$.

Fig. 5 Comparison of time-level history of flyover noise predicted with the LOPNOR tool and outdoor measurements.

Fig. 5 displays the comparison between time-level histories of flyover noise, computed using the present LO approach incorporating the acoustic effect of α_{disk}, and outdoor measurements. In all Cases, the general trend of the time-level history of flyover noise recorded by the outdoor measurements during the 30 s of flyover time is well captured by the LO predictions. The LO predictions exhibited good agreement with the measurement data when the aircraft was positioned directly above the microphone. This observation can be attributed to the directivity of propeller noise, with tonal noise predominating on the propeller rotation plane, while broadband noise prevails toward the propeller axis, as discussed in Yunus et al. [6]. Consequently, the greatest discrepancy occurs when the aircraft is farthest from the microphone, as the emission point on the noise sphere is farther from the propeller rotation plane and closer to the propeller axis, where broadband noise dominates (refer to illustration on the right panel of Fig. 1). Conversely,

when the aircraft flies directly overhead, the emission point on the noise sphere aligns with the propeller rotation plane, facilitating the most efficient radiation of tonal noise and resulting in minimal discrepancy.

The suitability of the LO approach for rapid analysis of FEPD aircraft noise during the early design phase is underscored by comparisons of both the source noise spectra and time-level history of flyover noise against outdoor measurements. This approach is deemed acceptable for predicting tonal noise of both constant altitude level flight and take-off flights.

V. Conclusion

This study introduces an LO approach that integrates an aerodynamic module based on BEMT with an acoustic module based on frequency-domain acoustic formulation for predicting the tonal noise of FEPD aircraft in outdoor environments. To determine the predominance of propeller noise and evaluate the negligible contribution of noise from other propeller-airframe interactions, HF CFD simulations focusing exclusively on the propeller geometry are conducted. Comparison between HF CFD simulation results and outdoor measurements indicates that the propeller constitutes the primary noise source within the tonal frequency range, with tonal peaks corresponding to harmonics of the BPF observed above the broadband component. In this frequency range, the impact of various aerodynamic interactions between the propeller and the airframe can be disregarded during constant altitude level flight. A comparison of LO predictions with and without considering the acoustic effect of non-zero angle of attack against measurement data demonstrates that incorporating the acoustic effect of non-zero angle of attack enhances prediction accuracy at higher harmonics.

The recommendation to focus efforts on devising quieter FEPD models, with a specific emphasis on targeting propeller noise, is supported by the results presented in this study. Furthermore, the reliability of the present LO approach in predicting tonal noise of FEPD aircraft, even under take-off flight conditions, is demonstrated. These outcomes strongly suggest that the current LO approach serves as a valuable tool for evaluating propeller noise during the early design phase.

References

[1] Antcliff, K., Borer, N., Sartorius, S., Saleh, P., Rose, R., Gariel, M., Oldham, J., Courtin, C., Bradley, M., Roy, S., et al., "Regional Air Mobility: Leveraging Our National Investments to Energize the American Travel Experience," Tech. rep., NASA, 2021.

[2] Schwab, A., Thomas, A., Bennett, J., Robertson, E., and Cary, S., "Electrification of aircraft: Challenges, barriers, and potential impacts," Tech. rep., National Renewable Energy Lab.(NREL), Golden, CO (United States), 2021.

[3] Huang, Z., Yao, H., Sjögren, O., Lundbladh, A., and Davidson, L., "Aeroacoustic analysis of aerodynamically optimized joined-blade propeller for future electric aircraft at cruise and take-off," *Aerospace Science and Technology*, Vol. 107, 2020, p. 106336.

[4] Kurtz, D., and Marte, J., "A review of aerodynamic noise from propellers, rotors, and lift fans," Tech. rep., NASA, 1970.

[5] Casalino, D., Grande, E., Romani, G., Ragni, D., and Avallone, F., "Definition of a benchmark for low Reynolds number propeller aeroacoustics," *Aerospace Science and Technology*, Vol. 113, 2021, p. 106707.

[6] Yunus, F., Grande, E., Casalino, D., Avallone, F., and Ragni, D., "Efficient low-fidelity aeroacoustic permanence calculation of propellers," *Aerospace Science and Technology*, Vol. 123, 2022, p. 107438.

[7] Drela, M., "XFOIL: An analysis and design system for low Reynolds number airfoils," *Low Reynolds Number Aerodynamics: Proceedings of the Conference Notre Dame, Indiana, USA, 5–7 June 1989*, Springer, 1989, pp. 1–12.

[8] Carroll, J., and Marcum, D., "Comparison of a blade element momentum model to 3D CFD simulations for small scale propellers," *SAE International Journal of Aerospace*, Vol. 6, No. 2013-01-2270, 2013, pp. 721–726.

[9] Morgado, J., Vizinho, R., Silvestre, M., and Páscoa, J., "XFOIL vs CFD performance predictions for high lift low Reynolds number airfoils," *Aerospace Science and Technology*, Vol. 52, 2016, pp. 207–214.

[10] Loureiro, E. V., Oliveira, N. L., Hallak, P. H., de Souza Bastos, F., Rocha, L. M., Delmonte, R. G. P., and de Castro Lemonge, A. C., "Evaluation of low fidelity and CFD methods for the aerodynamic performance of a small propeller," *Aerospace Science and Technology*, Vol. 108, 2021, p. 106402.

[11] McCrink, M. H., and Gregory, J. W., "Blade element momentum modeling of low-reynolds electric propulsion systems," *Journal of Aircraft*, Vol. 54, No. 1, 2017, pp. 163–176.

[12] MacNeill, R., and Verstraete, D., "Blade element momentum theory extended to model low Reynolds number propeller performance," *The Aeronautical Journal*, Vol. 121, No. 1240, 2017, pp. 835–857.

[13] Yunus, F., "Methodologies and algorithms for sound propagation in complex environments with application to urban air mobility: A ray acoustics approach," PhD thesis, Delft University of Technology, Delft, The Netherlands, September 2023. Available at https://research.tudelft.nl/en/publications/methodologies-and-algorithms-for-sound-propagation-in-complex-env.

[14] Hanson, D. B., "Helicoidal surface theory for harmonic noise of propellers in the far field," *AIAA journal*, Vol. 18, No. 10, 1980, pp. 1213–1220.

[15] Hanson, D. B., and Parzych, D. J., "Theory for noise of propellers in angular inflow with parametric studies and experimental verification," Tech. rep., 1993.

[16] Hanson, D., "Sound from a propeller at angle of attack: a new theoretical viewpoint," *Proceedings of the Royal Society of London. Series A: Mathematical and Physical Sciences*, Vol. 449, No. 1936, 1995, pp. 315–328.

[17] Kotwicz Herniczek, M. T., Feszty, D., Meslioui, S.-A., Park, J., and Nitzsche, F., "Evaluation of acoustic frequency methods for the prediction of propeller noise," *AIAA Journal*, Vol. 57, No. 6, 2019, pp. 2465–2478.

[18] Kvurt, A., and Stalnov, O., "From the Blade Geometry to Prediction of Tonal Noise Component in Hover," *28th AIAA/CEAS Aeroacoustics 2022 Conference*, 2022, p. 3076.

[19] Kvurt, A., Ruf, D., Hertzman, O., Stalnov, O., and Ben-Gida, H., "getPROP-A MATLAB Suite for Low-Signature Propeller Design, Analysis, and Optimization," *AIAA SCITECH 2023 Forum*, 2023, p. 0026.

[20] Hanson, D., "Noise radiation of propeller loading sources with angular inflow," *13th Aeroacoustics Conference*, 1990, p. 3955.

[21] Viterna, L., and Corrigan, R., "Fixed pitch rotor performance of large horizontal axis wind turbines,N83 19233,1981," Tech. rep., NASA, 1981.

[22] Leishman, G. J., *Principles of helicopter aerodynamics with CD extra*, Cambridge university press, 2006.

[23] Kotwicz Herniczek, M. T., Feszty, D., Meslioui, S.-A., and Park, J., "Applicability of early acoustic theory for modern propeller design," *23rd aiaa/ceas aeroacoustics conference*, 2017, p. 3865.

[24] Magliozzi, B., Hanson, D., and Amiet, R., "Propeller and propfan noise," *Aeroacoustics of flight vehicles: theory and practice*, Vol. 1, 1991, pp. 1–64.

[25] Elbers, N., "Assessment of an aircraft propeller noise model by verification and experimental validation," Masters thesis, Delft University of Technology, Delft, The Netherlands, December 2021. Available at https://repository.tudelft.nl/islandora/object/uuid:d566dd4b-b6ac-4b52-b05b-0e1391281936.

[26] Pipistrel, "PIPISTREL, Velis Electro," , accessed: 23.10.2023. URL https://www.pipistrel-aircraft.com/products/velis-electro/.

[27] EASA, "TYPE-CERTIFICATE DATA SHEET For Type Virus SW 121," , accessed: 23.10.2023. URL https://www.easa.europa.eu/en/document-library/type-certificates/aircraft-cs-25-cs-22-cs-23-cs-vla-cs-lsa/easaa573-virus-sw-121.

[28] FARO, "FARO Quantum max arms," , accessed: 26.10.2023. URL https://www.faro.com/en/Products/Hardware/ScanArms.

[29] Ffowcs Williams, J. E., and Hawkings, D. L., "Sound generation by turbulence and surfaces in arbitrary motion," *Philosophical Transactions of the Royal Society of London. Series A, Mathematical and Physical Sciences*, Vol. 264, No. 1151, 1969, pp. 321–342.

[30] Casalino, D., "An advanced time approach for acoustic analogy predictions," *Journal of Sound and Vibration*, Vol. 261, No. 4, 2003, pp. 583–612.

[31] Farassat, F., and Succi, G. P., "The prediction of helicopter rotor discrete frequency noise," *In: American Helicopter Society*, 1982, pp. 497–507.

[32] Carley, M., "The structure of wobbling sound fields," *Journal of Sound and Vibration*, Vol. 244, 2001, pp. 1–19. https://doi.org/10.1006/jsvi.2000.3451.

[33] "The radiation of sound from a propeller at angle of attack," *Proceedings of the Royal Society of London. Series A: Mathematical and Physical Sciences*, Vol. 431, No. 1882, 1990, pp. 203–218.

[34] Yunus, F., Casalino, D., Avallone, F., and Ragni, D., "Toward inclusion of atmospheric effects in the aircraft community noise predictions," 2021.